A Point Source Survey of M31 with the Spitzer Space Telescope

Jeremy Mould

School of Physics, University of Melbourne, Vic 3010, Australia

Pauline Barmby

Department of Physics & Astronomy, University of Western Ontario, 1151 Richmond St, London ON N6A 3K7, Canada

Karl Gordon

Space Telescope Science Institute, 3700 San Martin Drive, Baltimore, MD 21218

S.P. Willner & M.L.N. Ashby

Harvard Smithsonian Center for Astrophysics, 60 Garden St, Cambridge, MA 02138

R.D. Gehrz, Roberta Humphreys, & Charles E. Woodward

Department of Astronomy, University of Minnesota, 116 Church St SE, Minneapolis, MN 55455

ABSTRACT

We explore the stellar population of M31 in a Spitzer Space Telescope survey utilizing IRAC and MIPS observations. Red supergiants are the brightest objects seen in the infrared; they are a prominent evolutionary phase. Due to their circumstellar envelopes, many of these radiate the bulk of their luminosity at IRAC wavelengths and do not stand out in the near infrared or optically. Going fainter, we see large numbers of luminous asymptotic giant branch stars, many of which are known long period variables. Relative to M33 the AGB carbon star population of M31 appears sparse, but this needs to be spectroscopically confirmed.

Subject headings: galaxies: individual (M31) – galaxies: stellar content

1. Introduction

The disk and bulge of M31 were first resolved into stars by Hubble (1936) and Baade (1944), respectively. Since then, many optical surveys have been carried out, including those of Hubble and Sandage (1953), Baade and Swope (1963), Hodge (1976), Berkhuijsen et al. (1988), Magnier et al. (1992), Mochjeska et al. (2001) and Massey et al. (2006). More recent papers that included spectra and optical and near-infrared photometry of individual stars are Humphreys (1979), Humphreys et al. (1988), Humphreys, Massey, & Freedman (1990), Herrero et al. (1994) and Massey (1998). Near-infrared point-source photometry of M31 has been hampered by the lack of large-format detectors; for example, the recent work of Olsen et al. (2006) covers only a small portion of M31. The 2MASS Large Galaxy Atlas (Jarrett et al. 2003) presented integrated photometry of M31, but no galaxy-wide assessment of the M31 point source population has been published.

Spitzer Space Telescope characterization of the point source population of other Local Group galaxies includes the Large Magellanic Cloud (Blum et al. 2006), M33 (Verley et al. 2007; McQuinn et al. 2007), and NGC 6822 (Cannon et al. 2007). Other Local Group dwarfs studied include IC1613 and the WLM galaxy (Jackson et al. 2007a,b, 2006). The Andromeda galaxy, M31, presents a unique opportunity to study stellar evolution at a chemical composition similar to that of the Milky Way. The red giant branch was resolved in V & I by Mould & Kristian (1986), and the brightest evolved stars have been studied by Massey (1998). However, an infrared survey of point sources in M31 has awaited the arrival of the Spitzer Space Telescope (Werner et al. 2004; Gehrz et al. 2007) and 2MASS (Jarrett et al. 2003).

In the mid-infrared, integrated measurements of M31 have been made by IRAS (Habing et al. 1984; Xu & Helou 1996), COBE/DIRBE (Odenwald et al. 1998), MSX (Kraemer et al. 2002) and *Spitzer* (Gordon et al. 2006; Barmby et al. 2006). With the aim of reaching stars with the most significant mass loss rates this paper presents a point source survey with the IRAC (Fazio et al. 2004) and MIPS (Rieke et al. 2004) cameras. We also utilize the 2MASS survey in order to include shorter wavelengths. We present extensive tables, giving positions of the sources we identify, to enable follow-up of these observations.

2. IRAC Survey

The IRAC data and reduction are described in Barmby et al. (2006). Briefly, the central $1\overset{\circ}{.}6 \times 0\overset{\circ}{.}4$ of M31 was imaged to a depth of six 12-second frames per position, and the outer area to a size of $3\overset{\circ}{.}7 \times 1\overset{\circ}{.}6$ by four 30-second frames per position. The survey was

part of the Spitzer Cycle 3 program (Program Identification 3126). The data analyzed here were produced by version 14 of the Spitzer Science Center (SSC) pipeline; compared to the version 11 and 12 data used by Barmby et al. (2006), the newer version is expected to have more accurate pointing refinement for the individual frames. The 3000 individual frames per channel were combined with the MOPEX software to create mosaics with a pixel scale of $0\farcs86$, sub-sampling the native IRAC pixel scale by a factor of $\sqrt{2}$ to better sample the point spread function (FWHM $\sim 1\farcs9$).

The saturation limits given in the IRAC Data Handbook [1] correspond to Vega magnitudes of $(9.9, 9.3, 6.7, 6.8)$ for 12-second frames and $(10.8, 10.4, 7.7, 7.8)$ for 30-second frames for the Spitzer 3.6, 4.5, 5.8, 8 μm bands respectively. The sensitivity can be estimated using the SSC Performance Estimation Tool (http://ssc.spitzer.caltech.edu/irac/sens.html); assuming a medium background, the 5σ point source detection limits correspond to Vega magnitudes of $(19.0, 18.0, 15.6, 14.9)$ for six 12-second frames and $(19.6, 18.5, 16.0, 15.2)$ for four 30-second frames. However, point source photometry in the vicinity of M31 is affected by crowding and at longer wavelengths by the diffuse ISM, and these values are presented as a guide only.

The IRAC flat-fields are derived from observations of the zodiacal light and observations of calibration stars to correct for the fact that the large-scale sensitivity pattern varies with spectral shape. Using the 'photometric correction' images from the Spitzer Science Center, we constructed correction mosaics and applied them to the M31 mosaics. We tested two different corrections for alternately red and blue sources and found that the effect was small. The magnitude changes for the red source correction are $(0.02, 0.0, 0.0, 0.0)$ in the sense that point sources become fainter and the scatter about this mean is $(0.16, 0.04, 0.02, 0.02)$. With the blue source correction stellar magnitudes in Table 1 become brighter by $(-0.11, -0.08, -0.06, -0.04)$. The scatter about these means is $(0.20, 0.13, 0.13, 0.10)$. Therefore, we have not implemented a correction of this type, as the effect is small, and the conclusions below are unaffected.

3. MIPS Survey

The MIPS resolution ranges from 6 arcsec at 24 μm to 40 arcsec at 160 μm. Gordon et al. (2006) described the MIPS program surveying M31, fit a stellar population plus dust grain model to the spectral energy distribution, and discussed the structure of M31 in terms of its interactions with M32 and NGC 205. Point sources were extracted from the 7 individual

[1] http://ssc.spitzer.caltech.edu/irac/sat.html

MIPS 24 μm AOR mosaics that together cover approximately 1×3 degrees centered on M31.

The point source extraction was done using the PSF-fitting program StarFinder (Dioliati et al. 2000) using a MIPS 24μm model PSF appropriate for stars (Engelbracht et al. 2007). This method of extracting point source photometry has been extensively tested on LMC Spitzer observations (Meixner et al. 2006) and found to produce high quality point source catalogs at 24 μm.

4. Stellar Photometry

Point spread functions (PSFs) were taken from the MOPEX[2] analysis release by the Spitzer Science Center. Sixteen realizations of the PSF differing in pixel phase were constructed for each of the IRAC channels at the survey pixel scale and combined with DAOPHOT (Stetson 1987). Two passes were made with the ALLSTAR PSF-fitting software for each of the four channels, yielding over a quarter of a million point sources at 3.6 μm with a detection threshold of 2.5σ. At 8.0 μm we detected 160,000 sources with the same threshold. Source lists were merged with the DAOMASTER program (Stetson 1992), using a 1 pixel matching radius. Calibrated following Reach et al. (2005), and using aperture corrections based on the PSFs, Figure 1 is the IRAC 2-color diagram for these objects. It resembles the equivalent diagram for the Large Magellanic Cloud (Meixner et al. 2006). Dusty evolved stars are offset from the origin in Figure 1. Objects with [5.8]–[8] > 1 are young stellar objects and show some concentration to the ring of star formation in M31 (Habing et al. 1984), as seen in Figure 2. Figure 3 compares the luminosity functions in the inner and outer parts of the galaxy.

An estimate of the foreground star and background galaxy contamination may be obtained by comparison with a survey such as SWIRE (Lonsdale et al. 2004). Its lowest galactic latitude field is ELAIS-N2; $b = +42°$, compared to M31's $b = -21.2°$. Its IRAC 2-color diagram is reproduced in Figure 4. The IRAC catalog in this field covers ~ 4.2 deg^2. To a magnitude limit of [3.6] = 17, there are 40,953 objects in the ELAIS-N2 catalog; scaled to the IRAC M31 area (3.08 deg^2), this corresponds to 29,895 objects, a tenth of the total to 17th mag in M31. The color distribution of the SWIRE sources extends further to the red in [5.8]–[8.0] than the IRAC M31 sources, but the M31 sources' color extends further to the red in [3.6]–[4.5]. The brighter M31 sources also extend further to the red in [3.6]–[8.0]. All of these properties of the color distributions are consistent with the M31 sources being dominated by stellar objects rather than galaxies, particularly at the faint end.

[2]http://ssc.spitzer.caltech.edu/irac/postbcd/mopex.html

Figure 5 is a color magnitude diagram (CMD) depicting massive star evolution in M31. Most of the stars fall on a strong vertical feature. These are main sequence and supergiant stars, together with significant contamination from foreground stars. The horizontal feature at [3.6] = 10 mag shows the growth of circumstellar envelopes radiating at 300–1000K. To enable follow-up of these objects, magnitudes for [3.6] < 11 mag are recorded in Table 1. M31 is only a 29% overdensity for 9 < K < 11 mag in the 2MASS point source catalog. (We determined this by catalog searches in the four cardinal directions around M31.) We therefore expect 1/1.29, i.e. 77 ± 6 %, of the entries in Table 1 to be foreground. Figure 6 shows the SWIRE control field. Scaling the 268 ELAIS-N2 catalog with [3.6] < 11 mag to the area of our M31 field, we expect 196 such objects. There are 426 stars in the M31 field with [3.6] < 11 and measured [8.0] mags. If we assume that foreground objects scale as cosec(b), the estimate of 196 foreground stars becomes 362, which provides an independent estimate of the percentage foreground contamination of 85 ± 7% . That is a 2σ detection of evolved stars in M31 with [3.6] < 11 mag.

The maximum luminosity [3.6] = 9.5 mag corresponds to $M_{\rm bol} \approx -11.9$ according to the supergiant bolometric corrections of Johnson (1966) for a distance of $m - M = 24.4$ mag (Huterer et al. 1995). This is a conservative estimate, as [3.6] = 9.5 mag exceeds the saturation limits noted in §2. Such high luminosities (1–2.5 × 10^6 $L_\odot$) are reached in the evolution of 120 $M_\odot$ stars (Chiosi & Maeder 1986).

The tip of the asymptotic giant branch (AGB) (Wood et al. 1983) at M31 lies at [3.6] > 14 mag: all the evolved stars shown in Figure 5 are supergiants. The positions of η Car and VY CMa are represented on the diagram, moved to the distance of M31. Data for these objects are from Smith et al. (2001), Polomski et al. (1999), and Whitelock et al. (1994). Most of the stars with [3.6] ≈ 10 are bluer than these objects: they are presumably in an earlier evolutionary phase of thickening circumstellar envelopes [3]. Figure 7 extends deeper into the CMD for M31. Although photometric errors become significant for [3.6] ∼ 17, we see a large number of AGB stars, stretching from the tip at 14.4 to the detection limit at 17 mag. Figure 8 is the corresponding SWIRE control field.

We carried out completeness tests by adding artificial stars to the [3.6] image. Completeness falls to 50% at [3.6] = 15.5 mag and drops to almost zero at 16.5 mag.

We cross-correlated our catalog with that of Massey et al. (2006). Over 87,000 matches were found within 1.6 arcsec, but only a handful of these have been spectroscopically classified. Indeed, only 11 of these matches are included in Table 1, and these are (with two

[3]RY Scuti is another case in point (Gehrz et al. 2001). It has [3.8] – [8.9] ≈ 2.9 mag, but is considerably fainter than η Car and VY CMa at 3.6μm.

exceptions) 21st and 22nd V mag stars. Luminous Blue Variables are also known in M31 (Szeifert et al. 1996), but these have K magnitudes between 13.9 and 17.6. Clearly, there are many stars representing the latest stages of evolution in the stellar population of M31 that are most prominent in the infrared.

We can also compare the CMD of M31 with that of M33 in Figure 9. McQuinn et al. (2007) plot the IRAC [3.6] – [8] color distribution by [3.6] magnitude in their figure 19. In M33 $M_{3.6} < -10$ consists of AGB stars without dust; the other two histograms are carbon stars with dust. We consider the carbon star frequency of M31 in the next section.

5. Spectral Energy Distributions

We cross-correlated our source catalog with the 2MASS Sky Survey (Skrutskie et al. 2006) using the OpenSkyQuery facility (http://openskyquery.net/Sky/skysite) of the National Virtual Observatory. Some 923 matches were found. To go deeper in the near infrared, we downloaded a catalog from the ancillary data products of the 2MASS Extended Mission. This derives from a set of special observations made at the end of 2MASS survey operations that used exposure times 6 times longer than the main survey. These measurements reach ∼1 mag deeper than the survey. We found 3110 matches with the 6 × catalog within a 1.6 arcsec radius.

Figure 10 is a CMD plotted from these matches. Following the deep JHK photometry of M33 by Cioni et al. (2008), the strong vertical feature with J–K < 1 and K < 14.5 is foreground, mixed with M supergiants. The broader vertical feature with K > 14.5 are M type AGB stars and stars with J–K > 1.36[4] are candidate carbon stars. The principal difference between M31 and M33, besides the fact that the UKIRT M33 photometry goes deeper, is that the branch of carbon stars at K = 16 mag (in Figure 2) of Cioni et al. (2008) is mostly absent, replaced by a dozen or so stars in M31 at K ≈ 14 mag. The product of third dredge up, carbon stars are harder to make in metal rich envelopes (Renzini & Voli 1981).

Blum et al. (2006) have classified stars in the SAGE survey of the Large Magellanic Cloud (Meixner et al. 2006) according to their position in the [3.6], J-[3.6] CMD. Figure 11 reproduces this classification for an LMC distance modulus of 18.5 (Mould et al. 2000). Supergiants are separated in color from AGB M stars, which are in turn separated from AGB

[4]As M31 is more metal rich than M33, this cutoff is probably redder in M31. E(J–K) is only 0.01 mag larger in M31 than M33 (Schlegel, Finkbeiner, & Davis 1998).

C stars. In the LMC this separation is clearly made into distinct concentrations in the Hess diagram, in which the RGB tip, the oxygen-rich and carbon-rich AGB branches are clearly visible. In M31 the IRAC/2MASS CMD is sparser and noisier, and additional dredge up may be required to overcome additional metallicity and make carbon stars. Classification based on Figure 10 may be indicative rather than exact, until spectroscopy can be obtained at $14 < [3.6] < 16$ and J–K ≈ 2.

Matching with 6× 2MASS allowed spectral energy distributions (SED) to be plotted from 1–8 μm. Foreground stars will tend to show photospheric SEDs. For those stars showing a mid-infrared excess (defined as a peak at 3.6 μm or beyond), we display SEDs in Figure 12 and magnitudes in Table 2. Three broad classes of sources are seen in Figure 12: (i) those that peak at 3.6 μm, (ii) sources with a longer wavelength excess, and (iii) relatively flat spectrum sources. The first class are consistent with rather warm circumstellar envelopes ($\sim$1000K); in class (ii) the envelope is cooler ($\lesssim$500K); class (iii) would be consistent with compact HII regions, supernovae remnants, or planetary nebulae, especially if the approximately flat spectrum extends to 24 μm (Verley et al. 2007). Omitted from Figure 12 are cases where DAOMASTER failed to match a star at an individual wavelength. There are approximately 20 such cases for which spurious peaks appear in the SED.

Bolometric corrections are not tabulated for stars as red as some of these objects. Integrating these SEDs from 1 – 10 μm, we obtain luminosities from 1 – 20 $\times$ 10^4 $L_\odot$ for those that are members of M31. The majority of these stars are AGB stars with circumstellar envelopes; there are 12 that are nominally supergiants ($M_{bol} < -7$), mostly with warm circumstellar envelopes. We cannot rule out that some of these stars may be late type dwarfs in the foreground.

6. Long Period Variables

The catalog was also cross-correlated with the long period variable (LPV) catalog of Mould, Saha, & Hughes (2004) which covers about half of the disk of M31. We found 831 sources within 2.5 arcsec of LPVs, triple the number that would have been expected by chance. The matches appear in Table 3 and comprise over 40% of the LPV catalog. Figure 13 is the IRAC 2-color diagram for LPVs and Figure 14 is a color magnitude diagram.

The distribution of points in Figure 14 is bounded by the limits of Mould, Saha & Hughes's photometry at J $\approx$ 18.5 and the present photometry [3.6] $\approx$ 17 mag. With $\langle K \rangle$ = 16.38 mag, these LPVs have $M_{bol} \approx -5$ and are AGB stars. This contrasts with the LMC and M33 which show significant numbers of supergiant LPVs with $M_{bol} < -7$ in addition to

their AGB population (Wood et al. 1983; Mould et al. 1990).

7. MIPS sources

Over 25,000 sources from 1 Jy to 0.2 mJy were extracted from the MIPS 24 μm image. Sources that are bright at 24 μm include HII regions, supernova remnants, and planetary nebulae (Verley et al. 2007). Nevertheless, cross-correlation with the brightest six magnitudes of the IRAC stellar catalog yielded 599 matches within 1 arcsec, and these are found in Table 4. Sixty matches would have been expected by chance. Figure 15 shows that that many of these matches fall on the dusty stars side of the IRAC-MIPS 2-color diagram, rather than the young stellar objects side (Meixner et al. 2006). J004258.15+410731.3 is 667 day period LPV 33133. J004031.89+410624.7 is 785 day period LPV 16094. J004029.18+404453.8 is 575 day period LPV 14023. These are 3 of the 20 longest periods in the LPV catalog. Their SEDs are shown in Figure 16. These can be compared with some of the brighter MIPS sources in Figure 17. These extreme period LPVs appear to show two components, a photospheric component, and a dust shell that is relatively cool compared with those illustrated in §5.

The luminosity function of 24 μm sources is illustrated in Figure 18. Brighter sources tend to be contained within M31's ring of star formation and are more likely to be compact HII regions or young stellar objects.

8. Conclusions

Our Spitzer Space Telescope survey reveals a rich population of evolved stars in M31. Although there is strong foreground contamination, supergiants are present as bright as $1-2.5\times10^6$ $L_\odot$. These evolve into stars with extensive circumstellar envelopes like η Carinae and VY CMa in the Milky Way. A number of the brightest supergiants at 3.6 μm are so red that they will be missed in optical surveys. We also resolve stars below the tip of the AGB to $M_{\rm bol} = -5$ mag. Many of these are LPVs, which also have dusty envelopes. Photometric candidates for AGB carbon stars are much fewer in M31 than M33, but spectroscopy is required to quantify this.

This work is based on observations made with the Spitzer Space Telescope, which is operated by the Jet Propulsion Laboratory, California Institute of Technology under a contract with NASA. Support for this work was provided by NASA through an award issued by JPL/Caltech. This work makes use of 2MASS data products, a joint project of the

University of Massachusetts and IPAC/Caltech, funded by NASA and NSF. In addition to DAOPHOT, this research has made use of IRAF, which is distributed by NOAO. NOAO is operated by AURA under a cooperative agreement with NSF.

REFERENCES

Baade, W. 1944, ApJ, 100, 137

Baade, W. and Swope, H. 1963, AJ, 68, 436

Barmby, P. et al. 2006, ApJ, 650, L45

Berkhuijsen, E., Humphreys, R., Ghigo, F., & Zumach, W. 1988, A&AS, 76, 65

Blum, R. et al. 2006 AJ, 132, 2034

Cannon, J. et al. 2007, ApJ, 652, 1170

Chiosi, C. & Maeder, A., 1986, ARA&A, 24, 329

Cioni, M.,-R. L. et al. 2008, A&A (in press) astro-ph 08051143

Diolaiti, E., Bendinelli, O., Bonaccini, D., Close, L., Currie, D., & Parmeggiani, G. 2000, A&AS, 147, 335

Engelbracht, C. W. et al. 2007, PASP, 119, 994

Fazio, G. G. et al. 2004, ApJS, 154, 10

Gehrz, R. D. et al. 2001, ApJ, 559, 395

Gehrz, R. D. et al. 2007, Rev. Sci. Instrum., 78, 11302

Gordon, K. et al. 2004, ApJS, 154, 215

Gordon, K. et al. 2006, ApJ, 638, L87

Habing, H. et al. 1984, ApJ, 278, L59

Herrero, A. et al. 1994, A&A, 287, 885

Hodge, P. 1976, Atlas of the Andromeda Galaxy, (Seattle: Univ. of Washington Press)

Hubble, E. 1936, "The Realm of the Nebulae", (New Haven: Yale Univ. Press)

Hubble, E. and Sandage, A. 1953, ApJ, 118, 353

Humphreys, R. 1979 ApJ, 234, 854

Humphreys, R. et al. 1988, AJ, 96, 1884

Humphreys, R., Massey, P. & Freedman, W. 1990 AJ, 99, 84

Humphreys, R. et al. 2006, AJ, 131, 2105

Huterer, D., Sasselov, D., & Schechter, P. 1995, AJ, 110, 2705

Jackson, D. et al. 2006, ApJ, 646, 192

Jackson, D. et al. 2007a, ApJ, 656, 818

Jackson, D. et al. 2007b, ApJ, 667, 891

Jarrett, T. et al. 2003, AJ, 125, 525

Johnson, H. 1966, ARA&A, 4, 193

Kraemer, K. et al. 2002, AJ, 124, 2990

Lee, M.G. et al. 2002, ApJ, 565, 959

Lonsdale, C. et al. 2004, ApJS, 154, 54

McQuinn, K. et al. 2007, ApJ, 664, 850

Magnier, E. et al. 1992, A&AS, 96, 379

Massey, P. 1998, ApJ, 501, 153

Massey, P. et al. 2006, AJ, 131, 2478

Meixner, M. et al. 2006, AJ, 132, 2268

Mochejska, B., Kaluzny, J., Stanek, K., & Sasselov, D. 2001, AJ, 132, 271

Mould, J. & Kristian J. 1986, ApJ, 305, 591

Mould, J. et al. 1990, ApJ, 349, 503

Mould, J., Saha, A., & Hughes, S. 2004, ApJS, 154, 623

Mould, J. et al. 2000, ApJ, 529, 786

Odenwald, S., Newmark, J.,& Smoot, G. 1998, ApJ, 500, 554

Olsen, K. et al. 2006, AJ, 132, 271

Polomski, E. et al. 1999, AJ, 118, 2369

Reach, W. et al. 2005, PASP, 117, 978

Renzini, A. & Voli, M 1981, A&A, 94, 175

Rieke, G. H. et al. 2004, ApJS, 154, 25

Schlegel, D., Finkbeiner, D., & Davis, M. 1998, ApJ, 500, 525

Skrutskie, M. et al. 2006, AJ, 131, 1163

Smith, N. et al. 2001, AJ, 121, 1111

Stetson, P. 1987, PASP, 99, 191

Stetson, P. 1992, in IAU Colloq. 136, Stellar photometry – Current techniques and future developments, ed C.J. Butler & I. Elliot, (Cambridge: CUP), p.291

Szeifert, Th. et al. 1996, A&A, 314, 131

Verley, S. et al. 2007, A&A, 476, 1161

Werner, M.W. et al. 2004, ApJS, 154, 1

Whitelock, P. et al. 1994, MNRAS, 270, 364

Wood, P., Bessell, M. & Fox, M. 1983, ApJ, 273, 99

Xu, C. & Helou, G. 1996, ApJ, 456, 152

Table 1. **Photometry of the infrared brightest stars**

#	RA (2000)	Dec	[3.6]	[4.5]	[5.8]	[8]
J003648.82+395625.7	9.20341	39.94046	10.87 7	10.82 5	10.80 2	10.71 3
J003659.17+400336.6	9.24653	40.06018	9.67 11	9.36 2	9.23 10	9.00 1
J003700.47+395031.8	9.25196	39.84217	10.26 5	10.07 3	10.02 5	9.88 2
J003700.75+401914.0	9.25311	40.32055	9.99 12	9.76 5	9.66 5	9.60 2
J003700.97+395619.2	9.25404	39.93867	10.18 18	10.79 21	12.12 40	11.19 30
J003708.35+403034.8	9.28479	40.50966	10.16 7	9.24 10	8.52 1	8.37 1
J003708.38+403032.4	9.28490	40.50901	10.33 7		11.03 11	11.24 10
J003708.54+394701.7	9.28557	39.78380	10.82 7	10.92 5	10.93 7	10.79 5
J003709.07+401450.0	9.28779	40.24722	10.07 10	9.93 5	9.87 3	9.77 1
J003709.53+403350.1	9.28970	40.56393	10.98 5	10.81 7	10.91 2	10.87 7
J003716.53+395705.7	9.31886	39.95158	9.78 7	9.58 5	9.61 1	9.43 1
...	...	...	...	...	...	...

Note. — Magnitudes are given together with an uncertainty in hundredths of a magnitude. Table 1 is published in its entirety in the electronic edition of the *Astrophysical Journal*. A portion is shown here for guidance regarding its form and content.

Table 2. **2MASS 6× matches**

#	RA (2000)	Dec	J	H	K	[3.6]	[4.5]	[5.8]	[8.0]
52	9.62906	40.30904	17.17	16.64	17.16	11.50	11.59	11.38	11.35
24	9.67014	40.47509	17.57	16.80	16.16	13.04	12.98	12.95	12.85
3	9.72386	40.49491	18.25	16.67	16.22	14.01	13.28	12.79	12.28
43	9.72643	40.62497	17.69	16.62	16.30	12.03	12.10	11.74	12.17
49	10.07809	40.60300	17.69	16.36	16.26	13.72	12.52	11.37	10.41
15	10.08307	40.56743	17.65	16.57	16.43	14.69	13.47	12.73	11.82
6	10.08431	40.67662	17.23	16.34	15.86	14.87	13.70	12.43	11.57
44	10.12849	40.70961	16.99	15.78	15.59	14.84	14.19	12.03	10.87
3075	10.13519	40.65016	16.37	16.20	15.32	15.18	14.90	11.97	10.16
2968	10.29796	41.13960	18.31	16.71	16.26	14.88	14.34	13.41	12.57
2947	10.33984	40.83079	17.83	16.77	16.26	14.45	14.04	11.49	9.66
...	...	...	...	...	...	...	...	...	...

Note. — Table 2 is published in its entirety in the electronic edition of the *Astrophysical Journal*. A portion is shown here for guidance regarding its form and content.

Table 3. **LPV matches**

MSH(2004) #	J	H	K	[3.6]	[4.5]	[5.8]	[8]
11009	18.05	16.84	16.38	16.03	15.93		
12008	17.12	16.07	16.03	16.23			
12022	17.63	17.40		16.17			
12026		17.42		16.45			
12034		17.30	17.20	16.68			
12040	17.90	17.03	16.74	15.84	15.60		
12041	18.43	17.08	17.54	15.80	15.98		
12042	17.59	17.03	17.47	16.00	14.99	14.36	13.10
12052		17.97		16.30			
12080	18.58			16.19			
12090	18.02	17.43	17.82	15.42			
12092		17.82	17.80	16.59			
13002	18.53	17.76	17.16	16.04	16.21		
13012	17.98	17.50	16.98	15.42	15.29	14.59	
13013	17.90	17.26	16.95	15.70	16.11		
13021	16.15	15.92	14.90	16.52			
...	...	...	...	...	...	...	...

Note. — Table 3 is published in its entirety in the electronic edition of the *Astrophysical Journal*. A portion is shown here for guidance regarding its form and content.

Table 4. **MIPS 24μ sources**

SSTM1M311 #	RA (2000)	Dec	[3.6]	[4.5]	[5.8]	[8]	[24]
J003921.35+402142.2	9.83898	40.36174	13.98	13.84	13.67	13.65	9.50
J004004.56+403844.1	10.01900	40.64558	14.62	14.55	13.98	13.51	10.42
J004014.35+404836.3	10.05983	40.81009	15.12	14.55	13.83	13.46	10.59
J004031.52+404126.6	10.13134	40.69073	15.86	15.49	12.64	10.75	5.63
J004032.94+403901.7	10.13728	40.65049	14.89	14.82	12.36	10.65	8.32
J004043.74+404326.6	10.18226	40.72406	15.51	15.20	14.35	12.88	10.70
J004046.28+403324.6	10.19284	40.55685	16.04	15.03	14.19	12.96	9.93
J004054.09+404606.5	10.22541	40.76847	15.68	15.58	14.39	12.43	10.11
J004055.89+404644.3	10.23291	40.77898	16.03	15.36		12.57	9.16
J004057.04+404935.8	10.23771	40.82663	15.75	15.22	14.30	13.92	9.65
J004059.78+403530.7	10.24912	40.59188	11.39	11.35	11.14	10.87	10.35
J004102.24+410432.1	10.25936	41.07561	15.73	15.51	12.80	10.77	8.31
J004104.65+405428.4	10.26940	40.90791	12.43	12.53	12.28	12.25	11.34
...	...	...	...	...	...	...	...

Note. — Table 4 is published in its entirety in the electronic edition of the *Astrophysical Journal*. A portion is shown here for guidance regarding its form and content.

Fig. 1.— IRAC 2-color diagram for sources in M31. The magnitudes are standard IRAC Vega magnitudes.

Fig. 2.— Distribution of sources with measured [8.0] magnitudes in M31. Sources with [5.8] – [8.0] > 1 are denoted by red triangles. The galaxy in the western "fin" of this plot is NGC 205. The northern major axis of M31 is to the left.

Fig. 3.— Source counts as a function of magnitude. The shaded area refers to the inner (deprojected) 9 kpc of M31. The unshaded area shows the full source counts.

Fig. 4.— IRAC 2-color comparison diagram for the ELAIS-N2 SWIRE field. Sources brighter than [3.6] = 17 mag are shown for comparison with Figure 1.

Fig. 5.— IRAC color magnitude diagram for sources in M31. The positions of two Galactic evolved stars are shown at M31's distance. Also shown is M33 Variable A (Humphreys et al. 2006). The distance modulus assumed for M33 is 24.52 mag (Lee et al. 2002).

Fig. 6.— IRAC color magnitude diagram for the ELAIS-N2 SWIRE control field.

Fig. 7.— Deep IRAC color magnitude diagram for sources in M31. This CMD extends to the AGB. Photometric errors ($\pm 1\sigma$) are displayed at the right of the figure.

Fig. 8.— Deep IRAC color magnitude diagram for the ELAIS-N2 SWIRE control field.

Fig. 9.— Color distribution as a function of magnitude for comparison with M33, see McQuinn et al. (2007). In M33 major peaks in the histograms indicate AGB stars without dust ([3.6]–[8] $\approx$ 0), carbon stars with dust ($0.5 \lesssim$ [3.6]–[8] $\lesssim 2.5$) and $M_{3.6} < -9$, and YSOs ([3.6]–[8] $\gtrsim$ 4).

Fig. 10.— CMD for the matches with 6× 2MASS.

Fig. 11.— CMD following the classification by Blum et al. (2006) of stars into supergiants (green), AGB oxygen-rich (blue), and AGB carbon-rich (red).

Fig. 12.— Spectral energy distributions for sources in 2MASS with mid-infrared excesses. The colored numbers refer to Table 2.

Fig. 13.— Two color diagram for M31's LPVs.

Fig. 14.— CMD for M31's LPVs.

Fig. 15.— IRAC-MIPS 2-color diagram for bright sources in M31 from Table 4. According to Meixner et al. 2006, young stellar objects lie on the right side of the dashed line.

Fig. 16.— Spectral energy distributions for 3 LPVs. The colored numbers are those of Mould, Saha, & Hughes (2003).

Fig. 17.— Spectral energy distributions for 5 bright 24μm sources in M31.

Fig. 18.— Luminosity function for 24μm sources. The red (dashed) histogram is for sources contained within M31's ring of star formation.

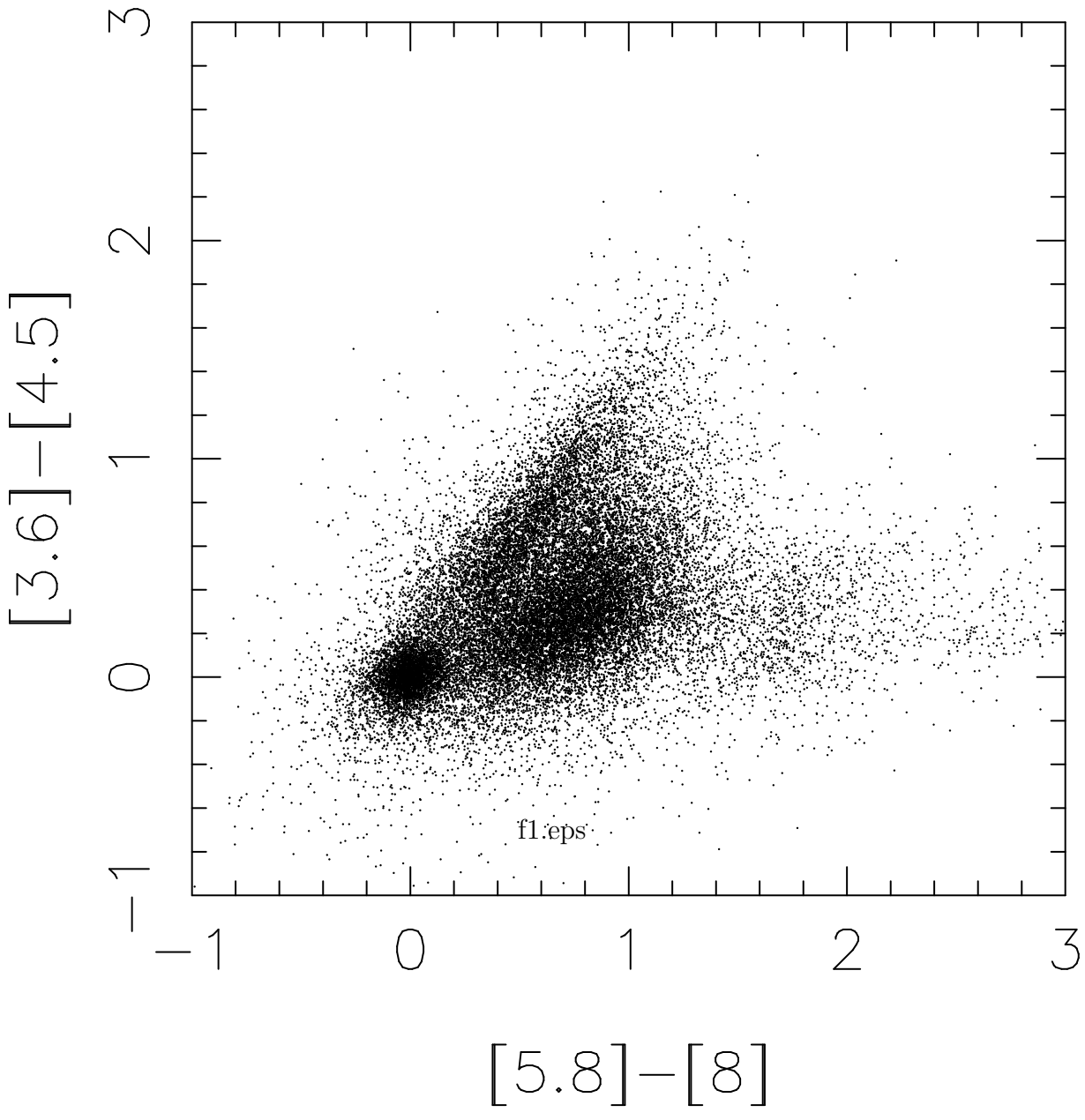
[3.6]−[4.5]
[5.8]−[8]
−1
0
1
2
3
f1.eps

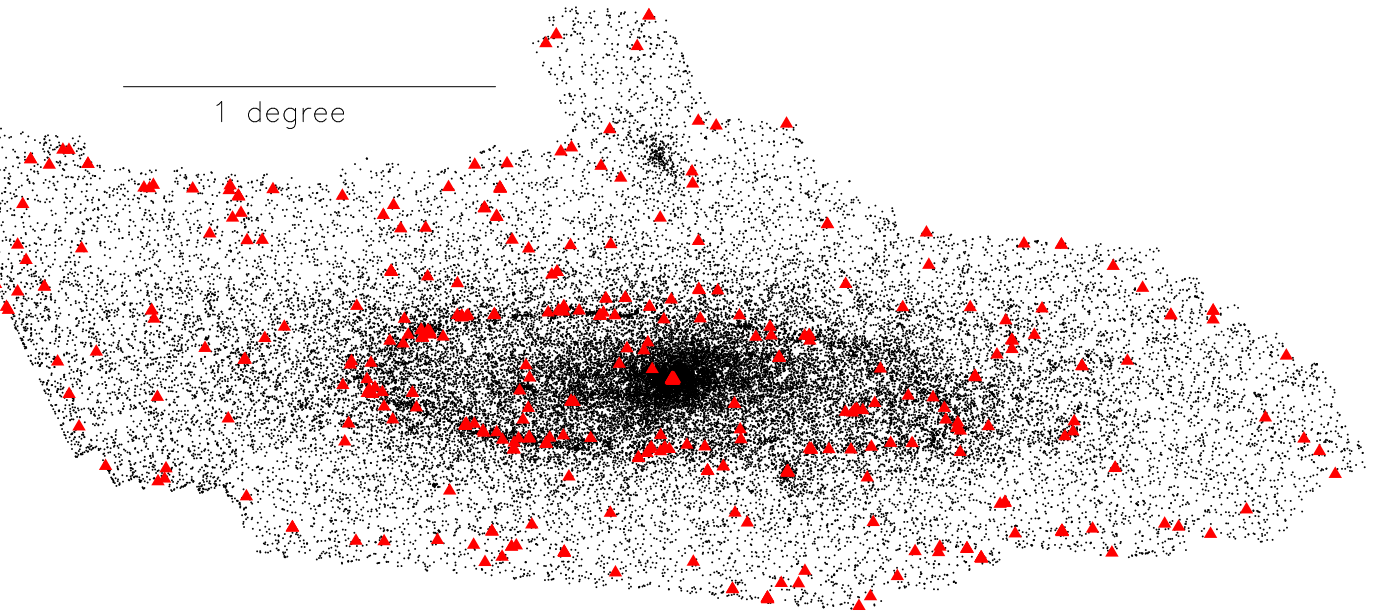

f2.eps

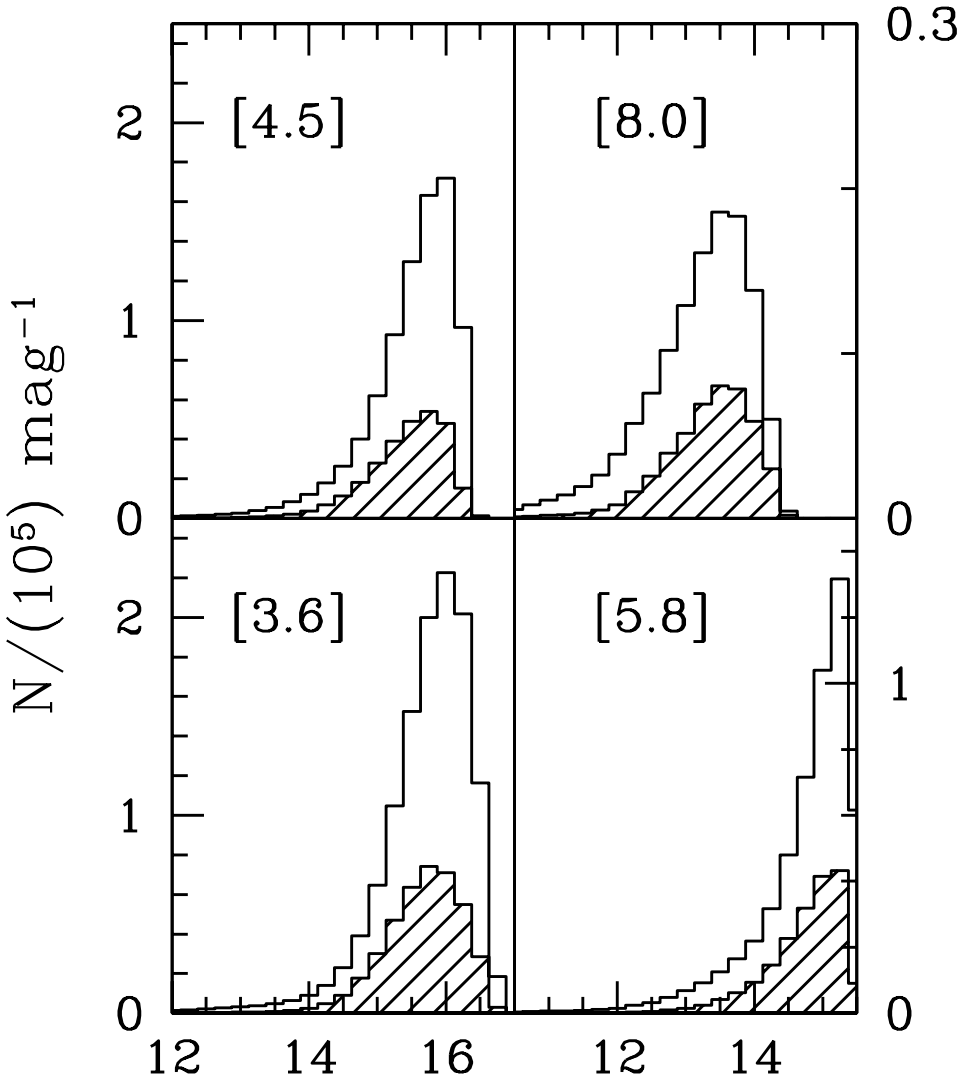

f3.eps

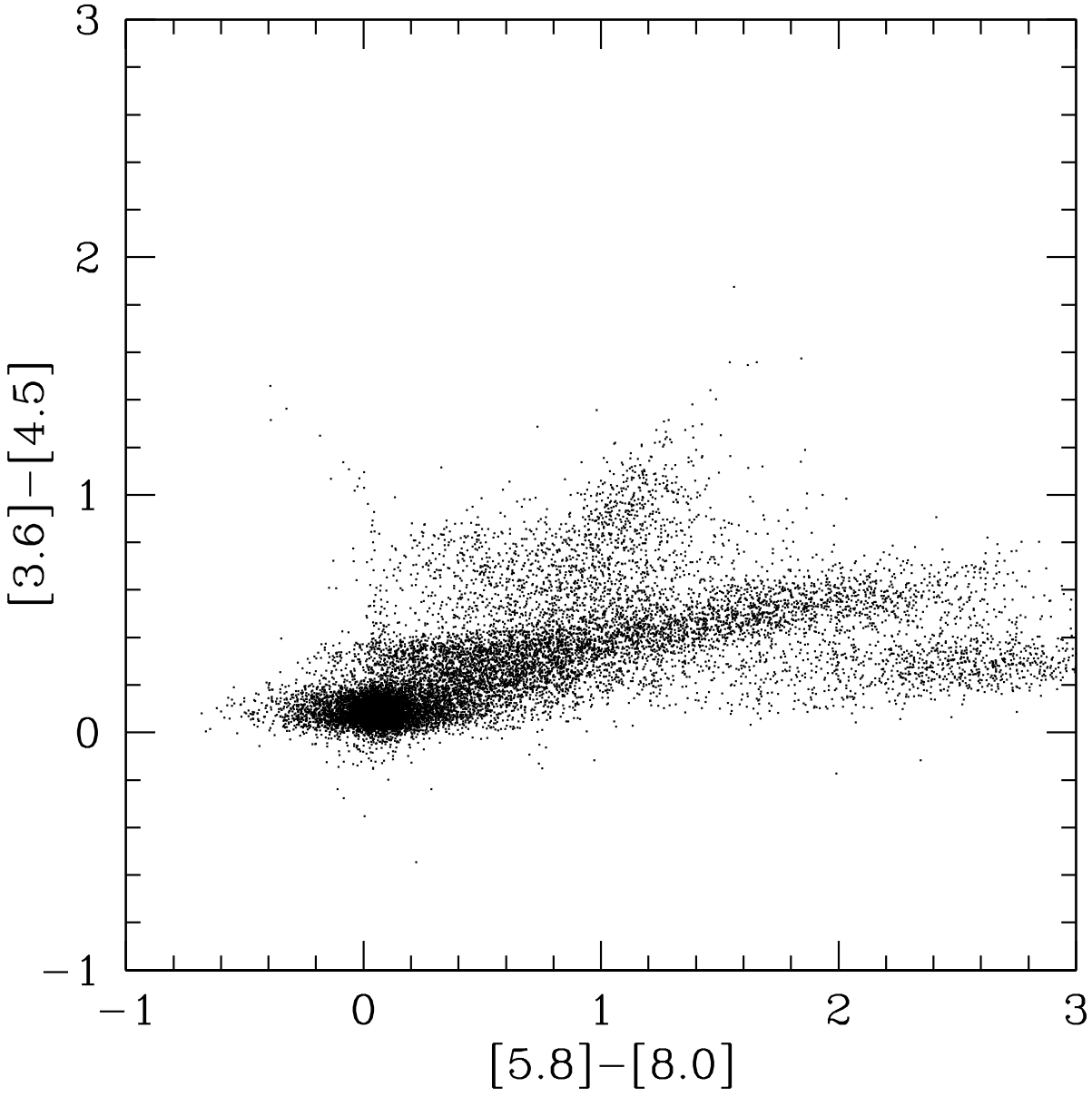

f4.eps

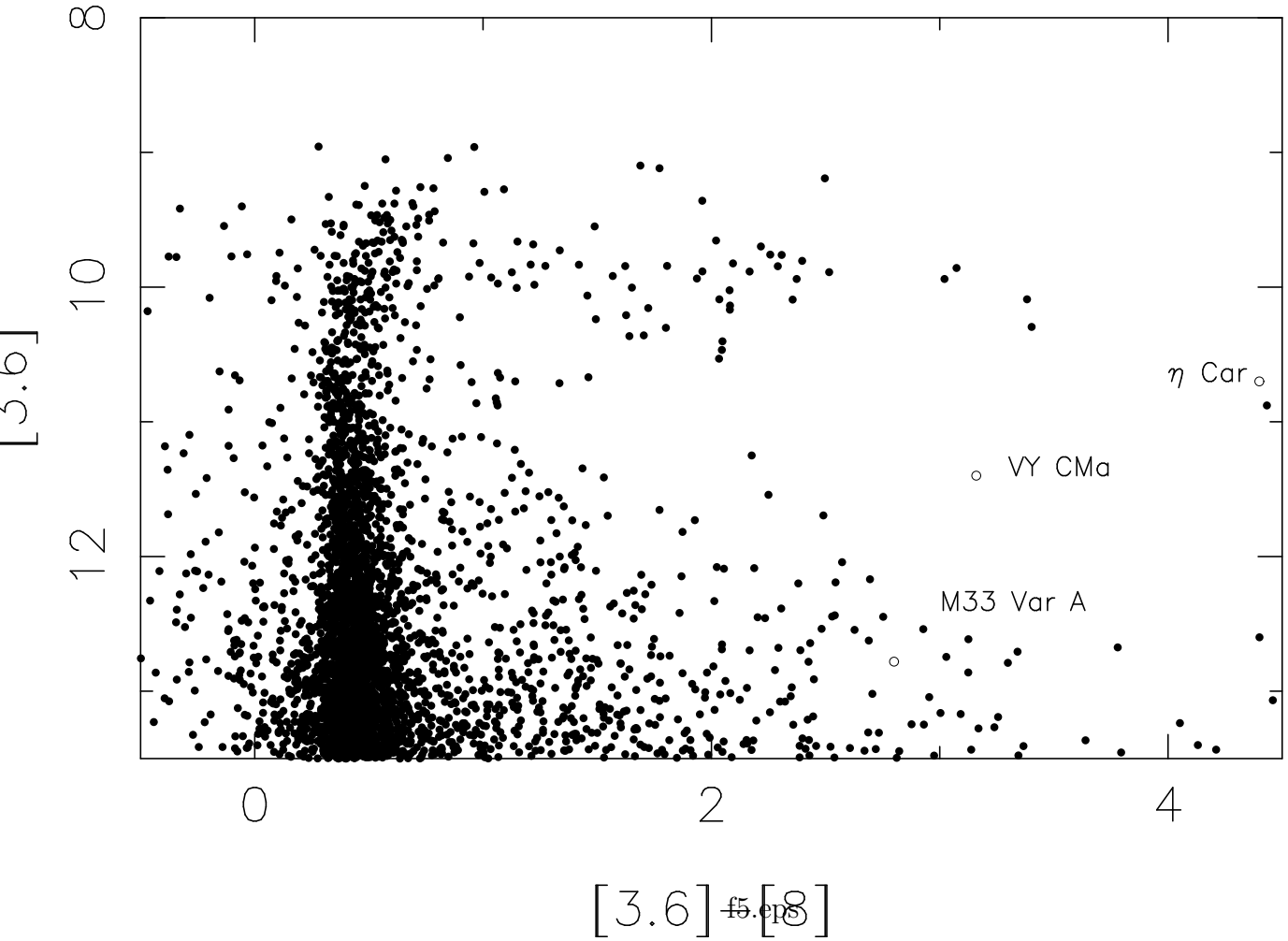

f5.eps

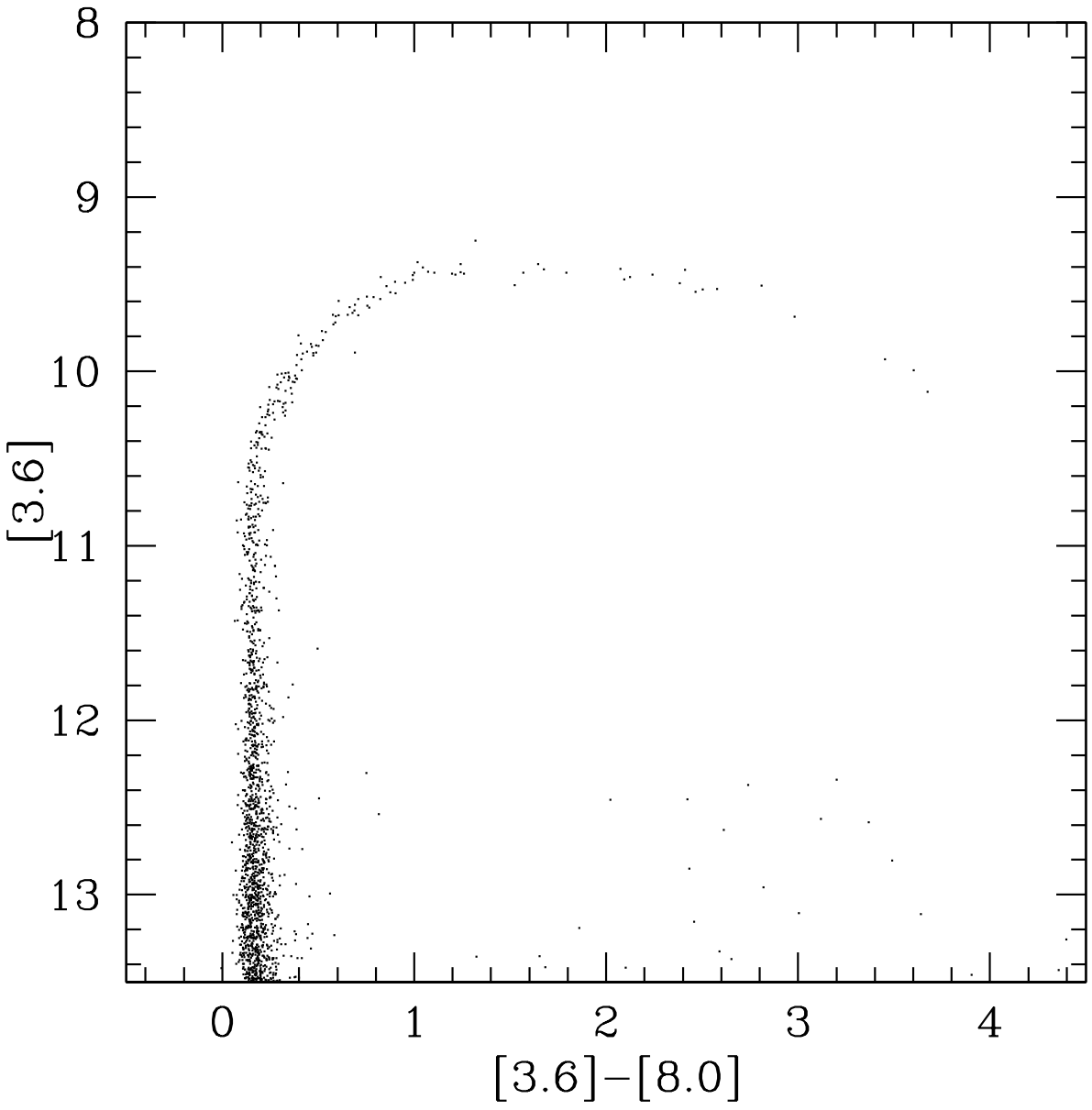

f6.eps

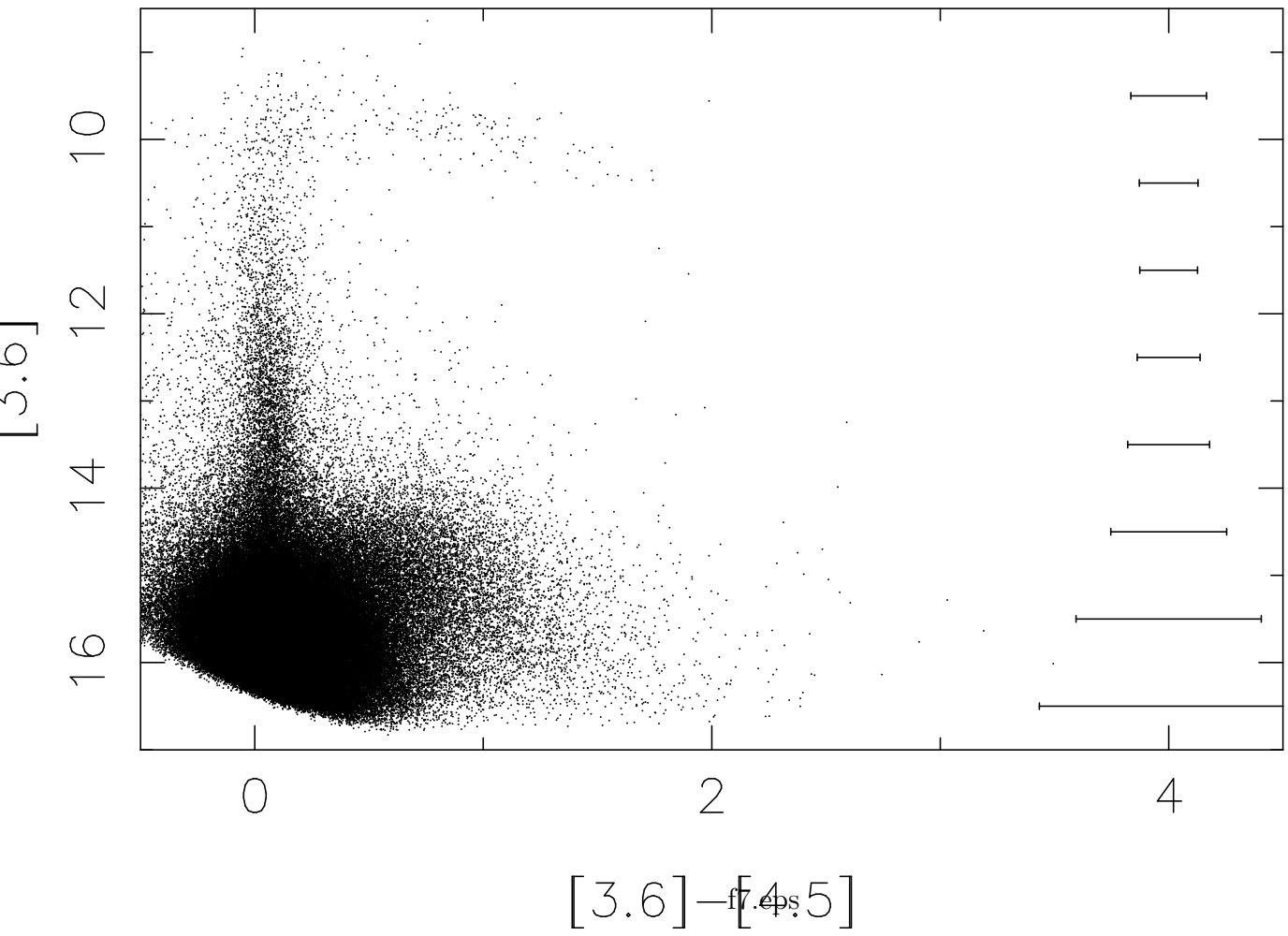

f7.eps

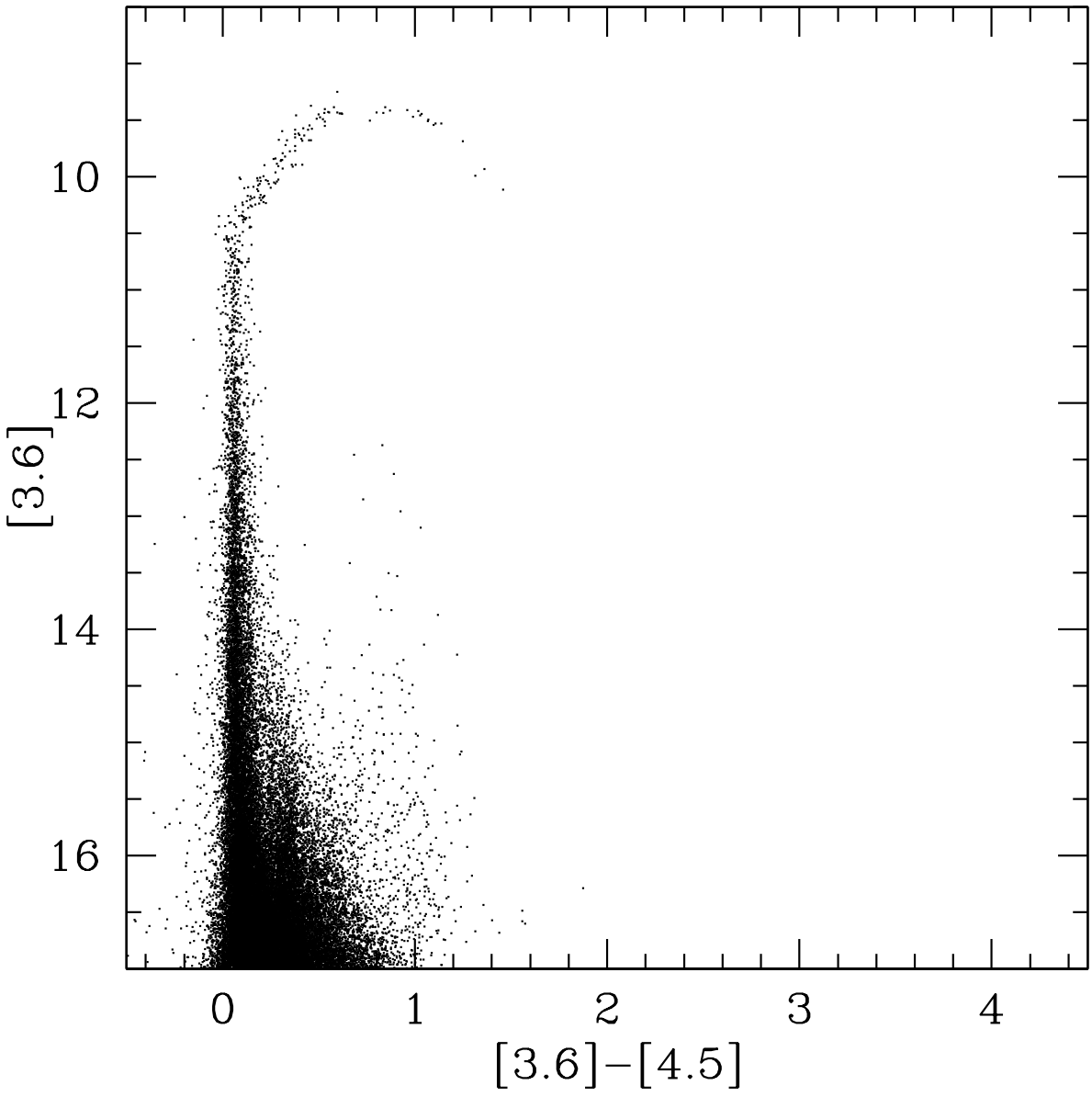

f8.eps

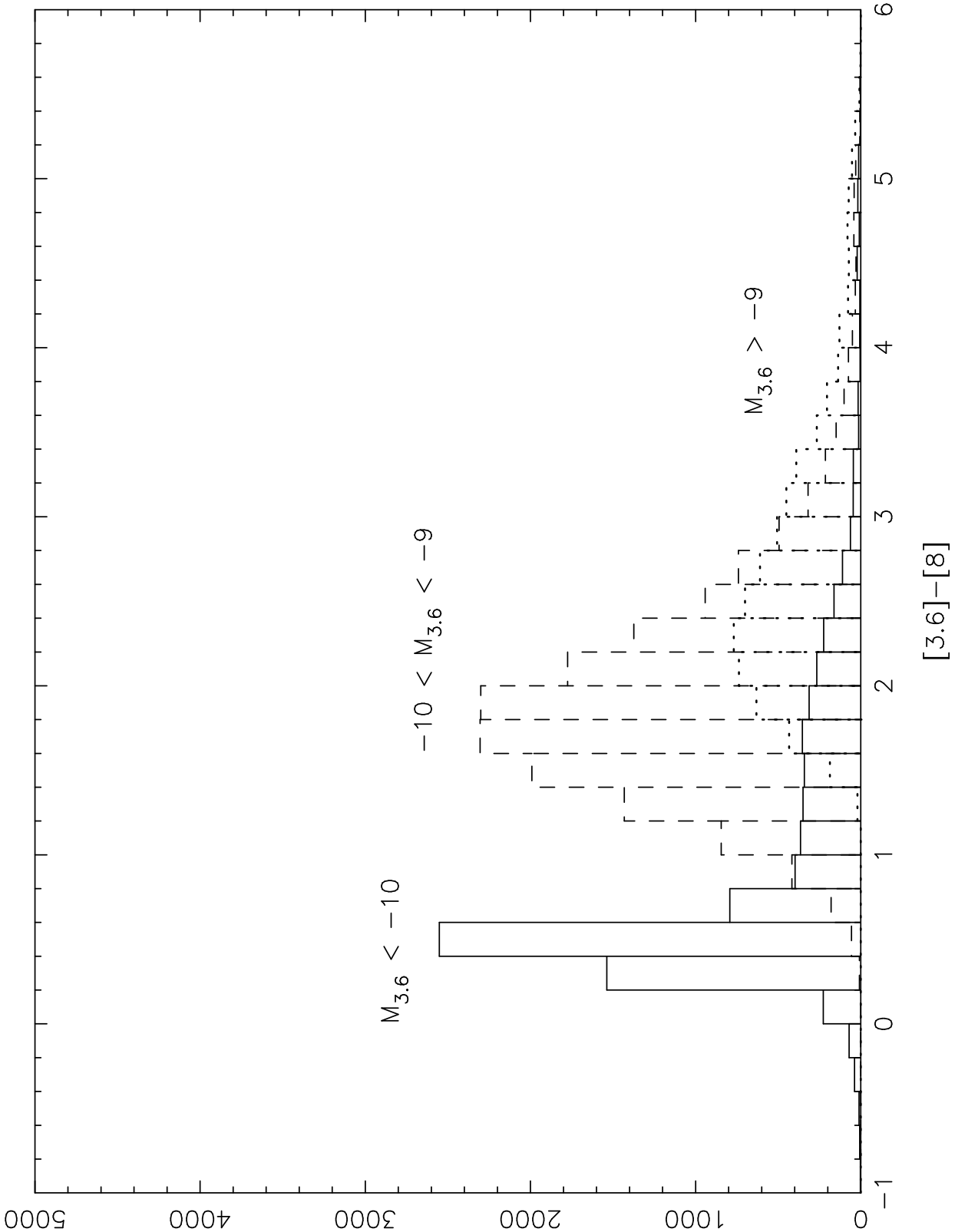

f9.eps

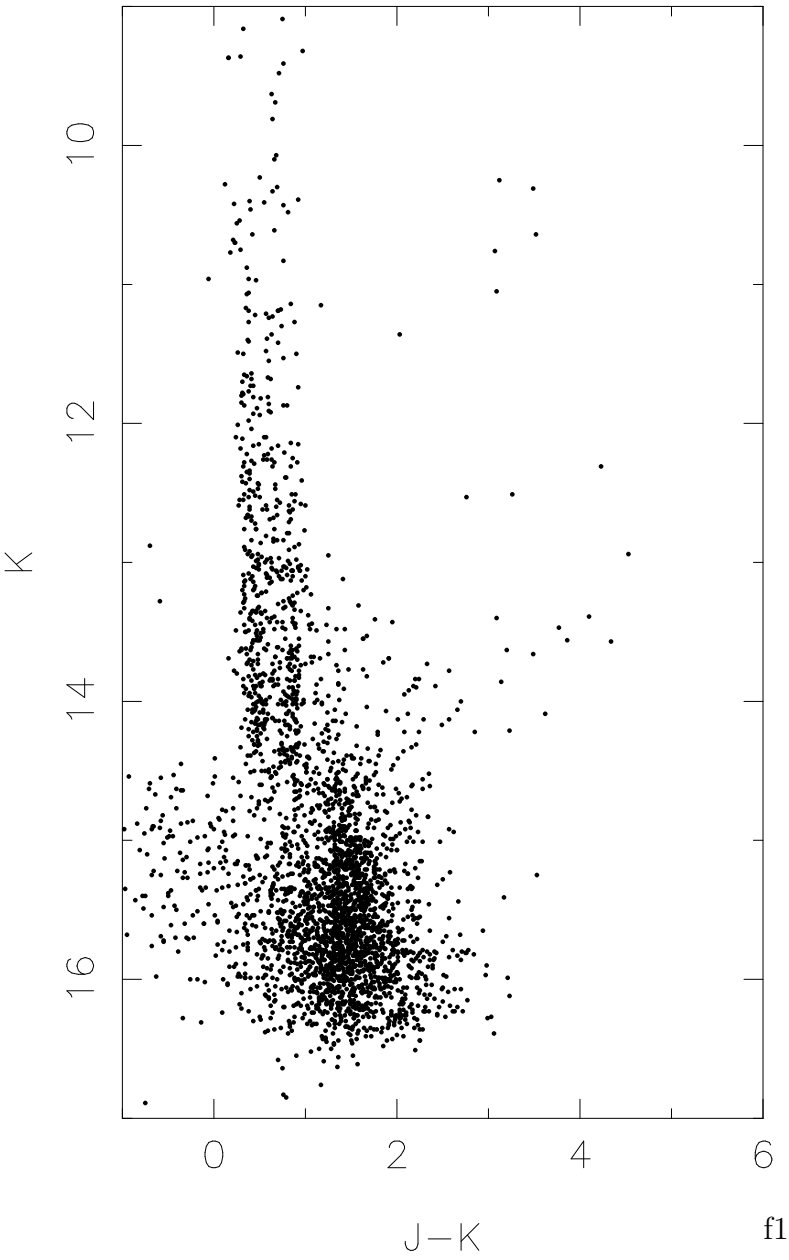

f10.eps

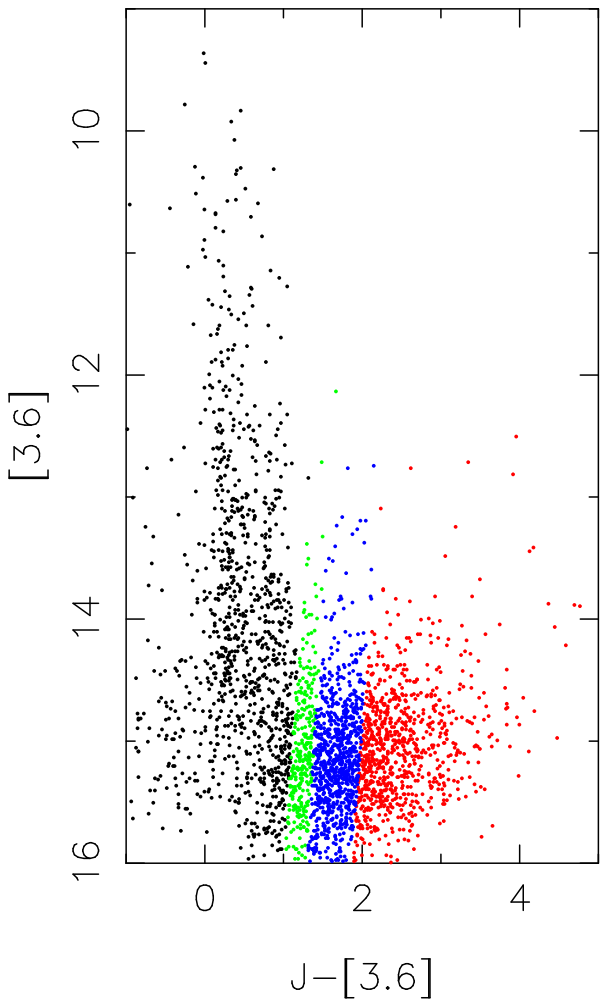

f11.eps

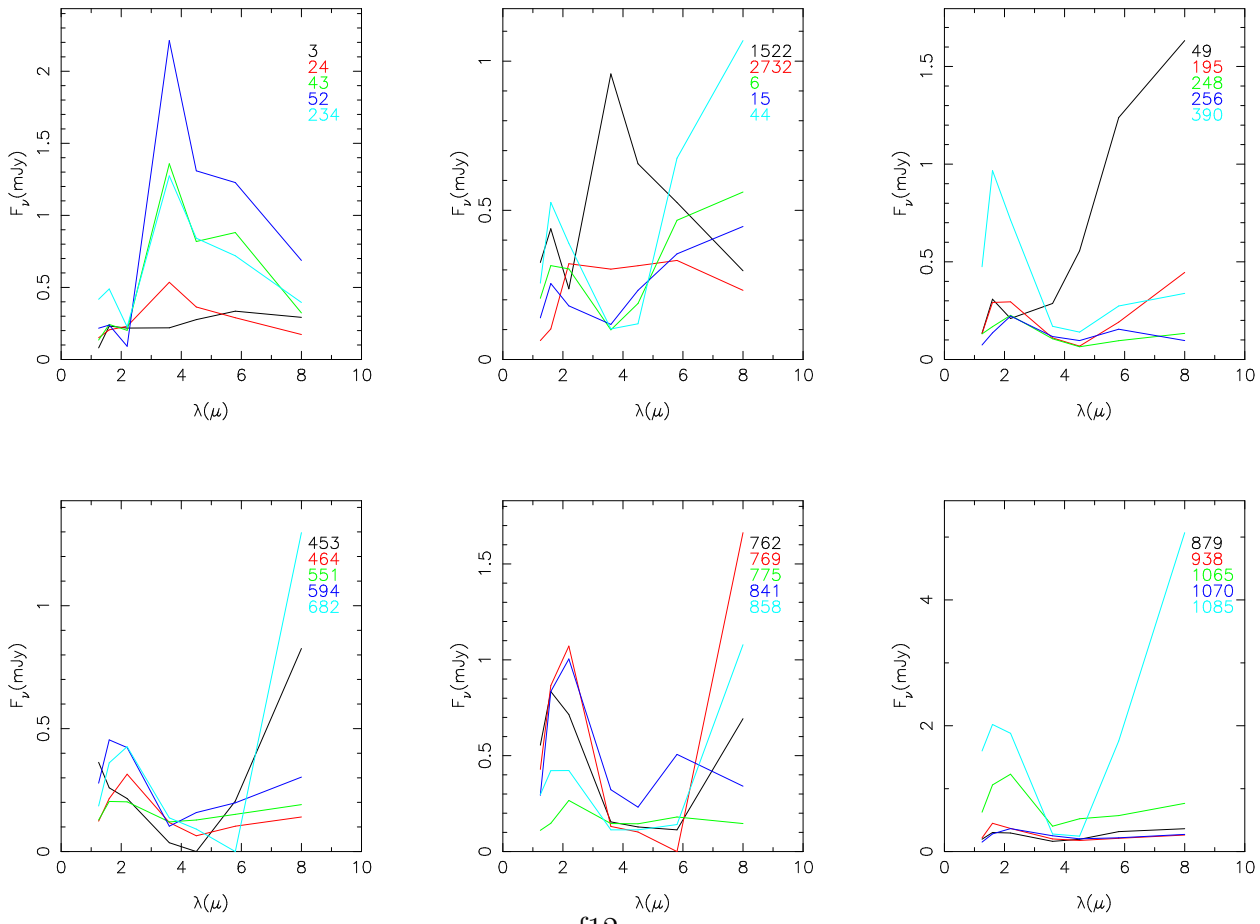
3
24
43
52
234
1522
2732
6
15
44
49
195
248
256
390
453
464
551
594
682
762
769
775
841
858
879
938
1065
1070
1085
F_ν(mJy)
λ(μ)

f12a.eps

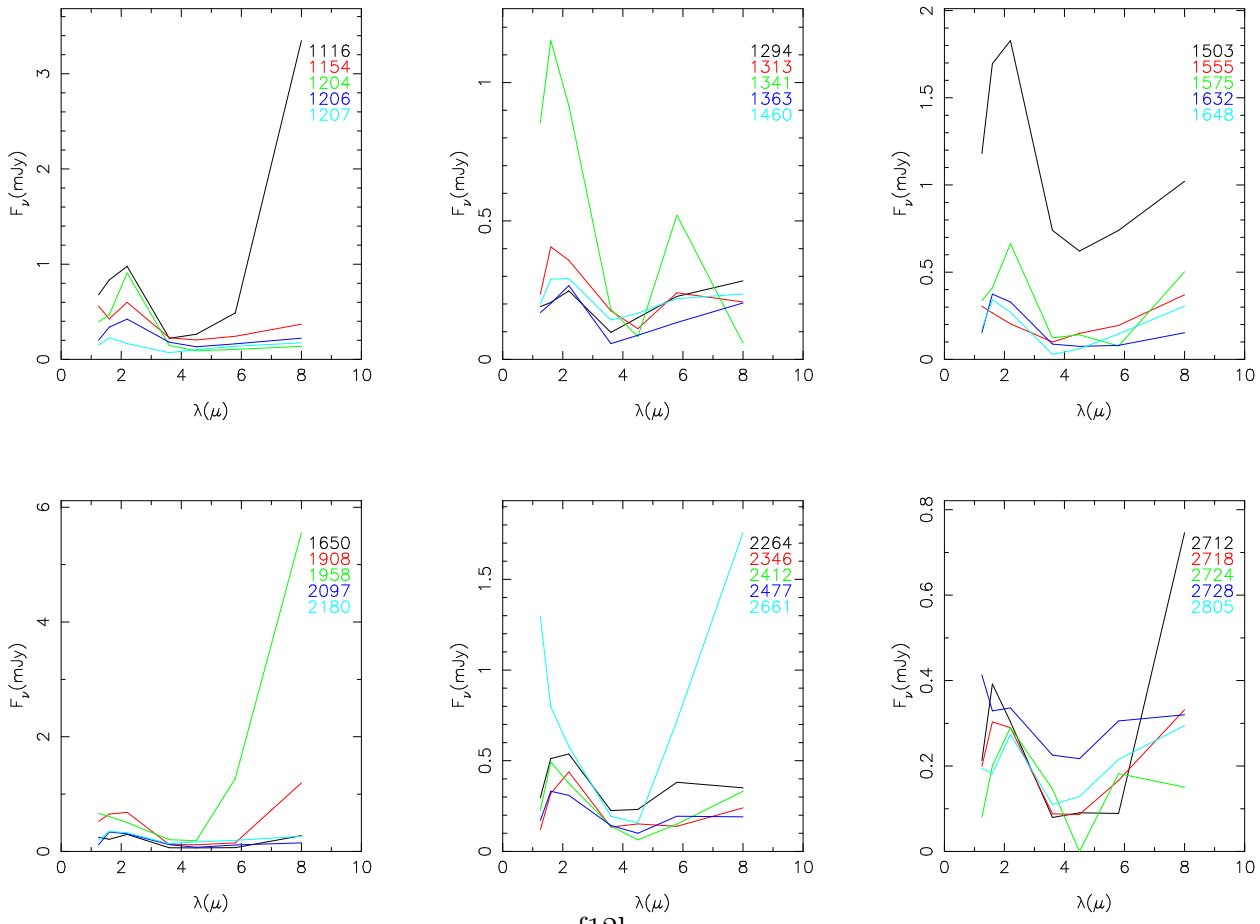
1116
1154
1204
1206
1207
1294
1313
1341
1363
1460
1503
1555
1575
1632
1648
1650
1908
1958
2097
2180
2264
2346
2412
2477
2661
2712
2718
2724
2728
2805
F_ν(mJy)
λ(μ)

f12b.eps

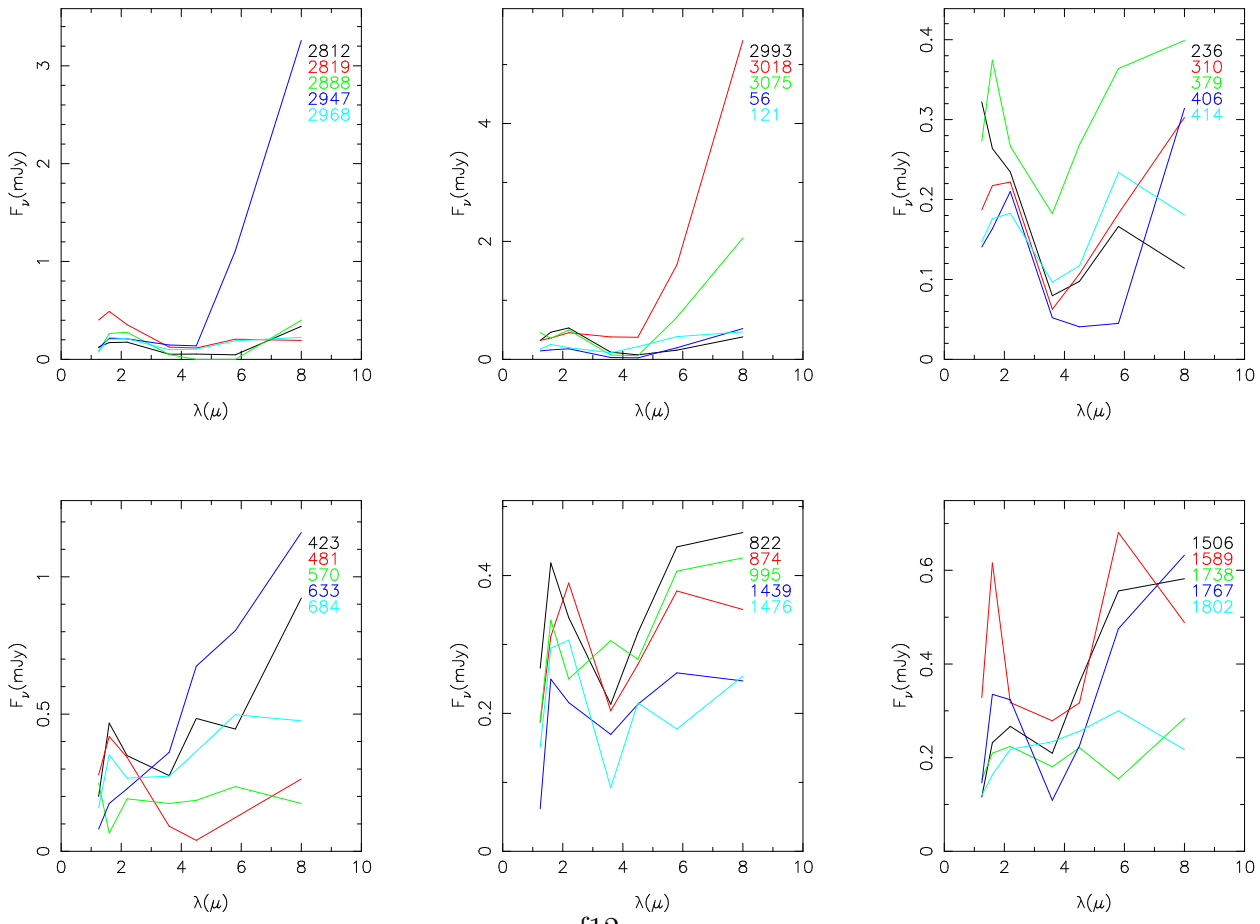
2812
2819
2888
2947
2968
2993
3018
3075
56
121
236
310
379
406
414
423
481
570
633
684
822
874
995
1439
1476
1506
1589
1738
1767
1802
F_ν(mJy)
λ(μ)

f12c.eps

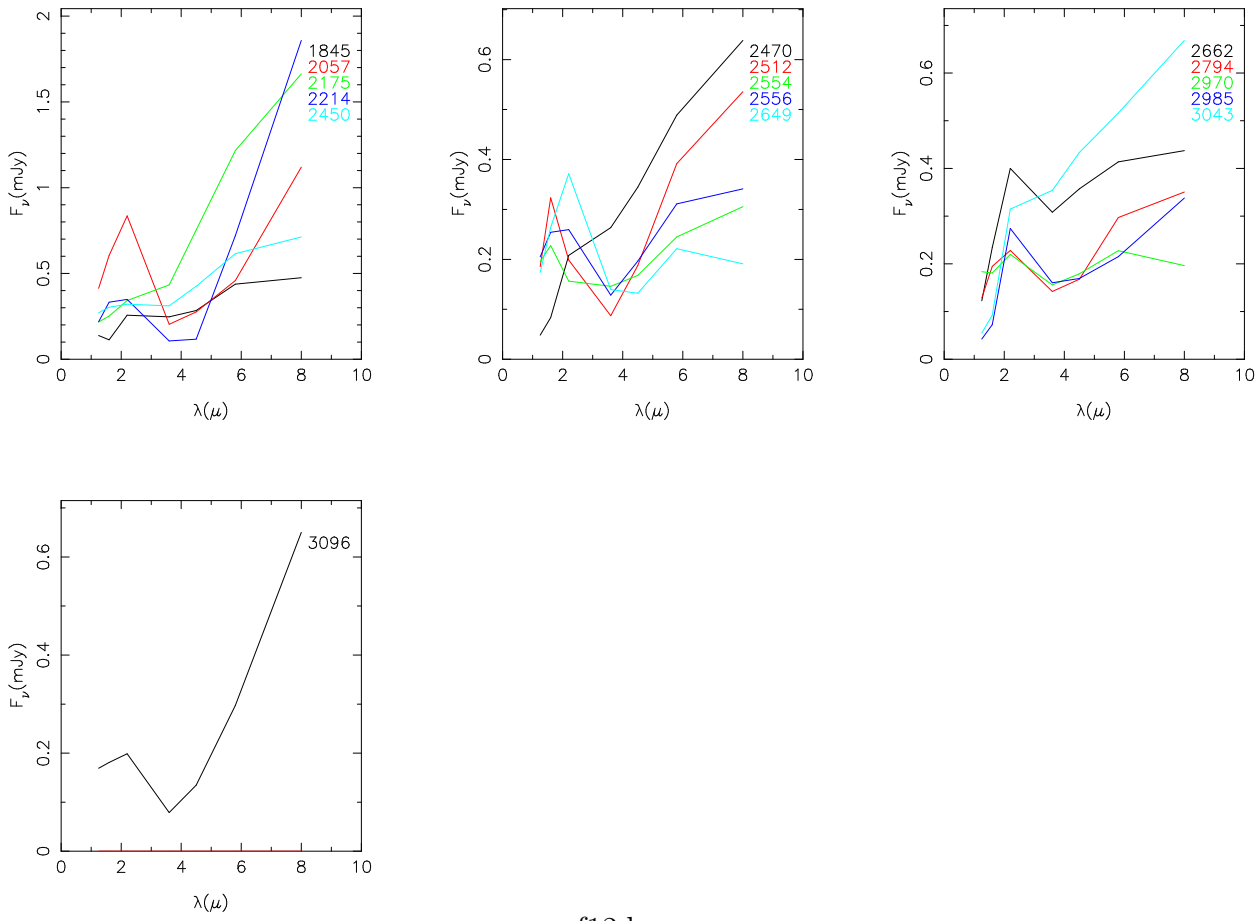
1845
2057
2175
2214
2450
2470
2512
2554
2556
2649
2662
2794
2970
2985
3043
3096
F_ν(mJy)
λ(μ)

f12d.eps

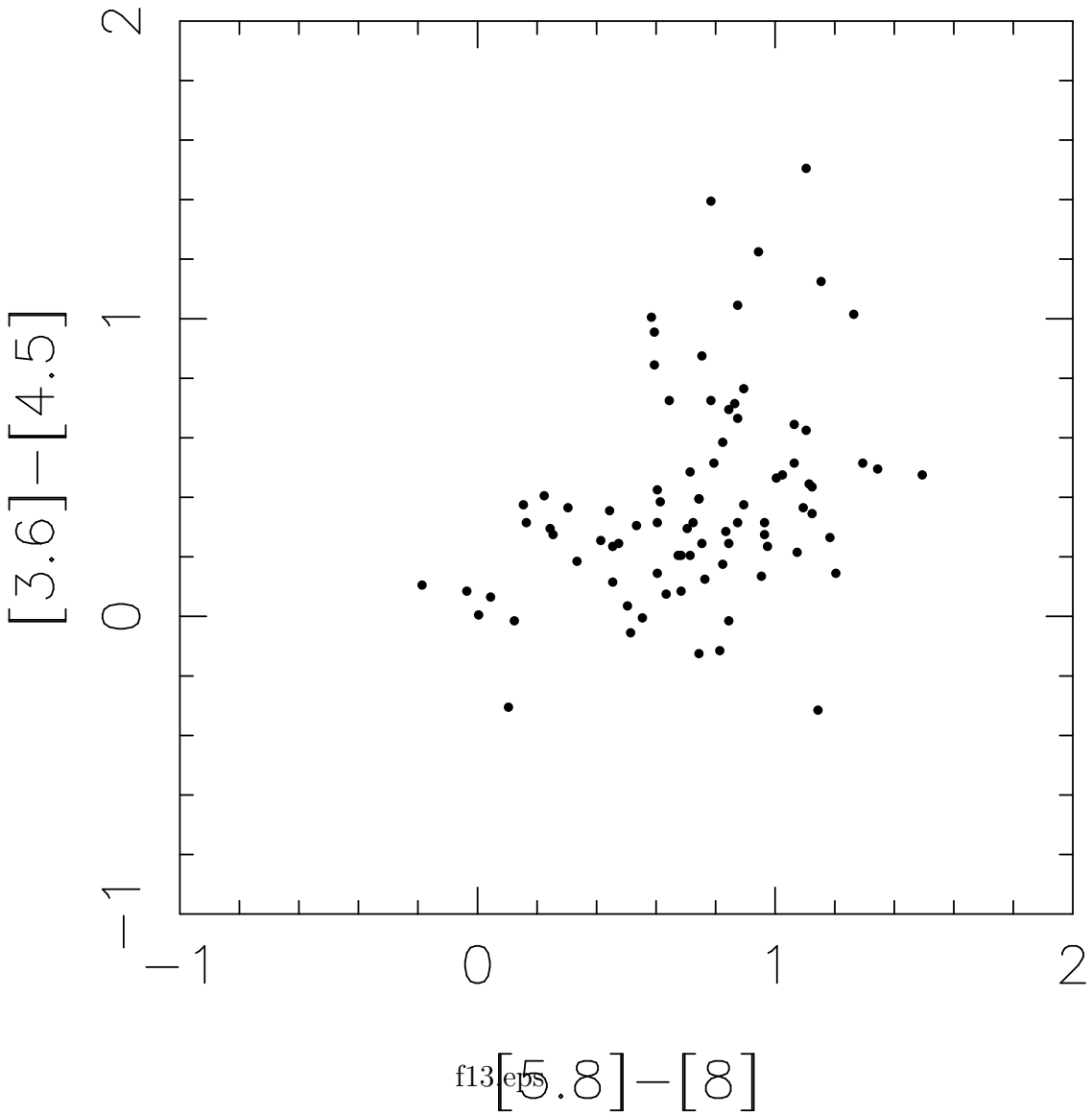

f13.eps

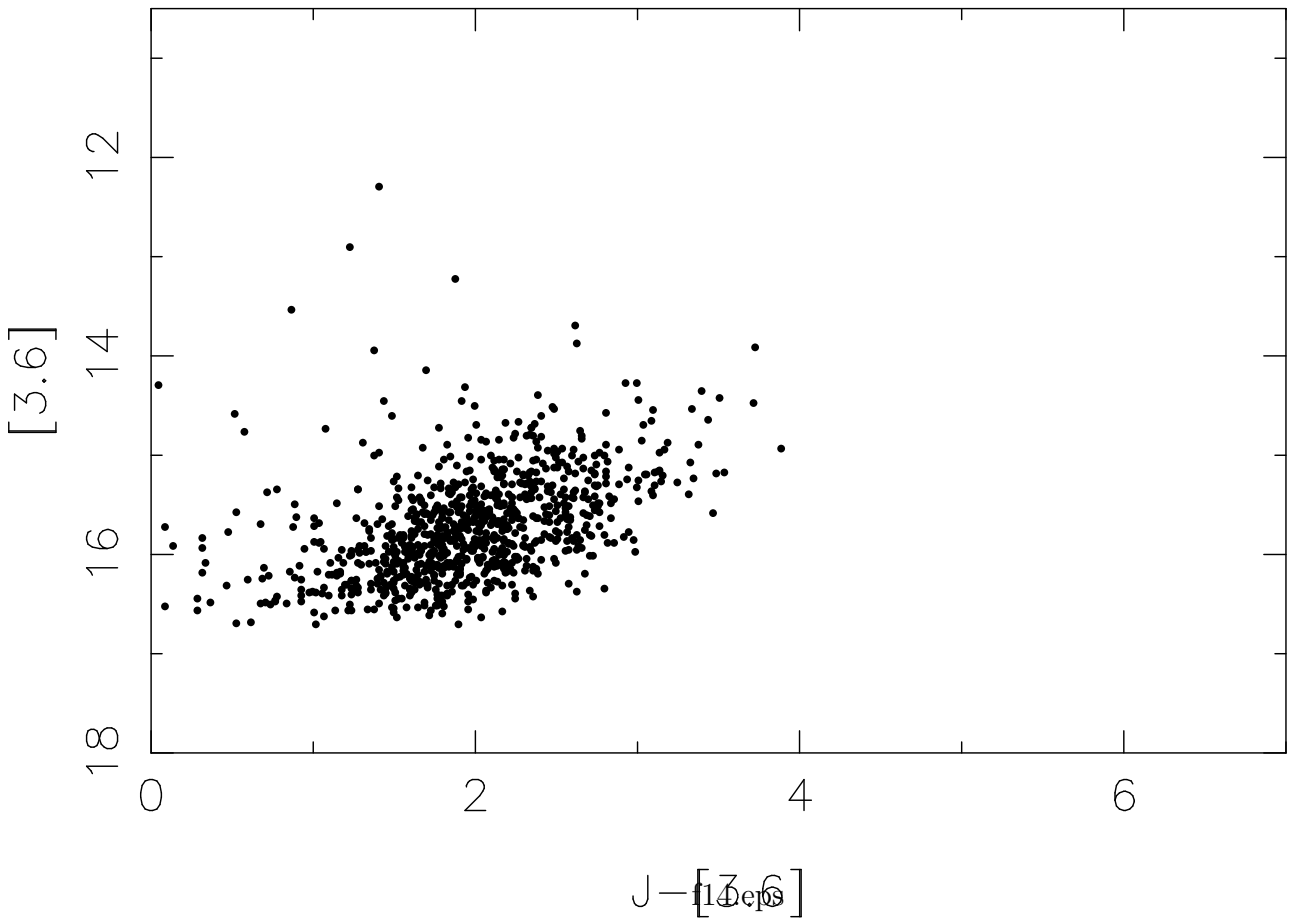

fig14.eps

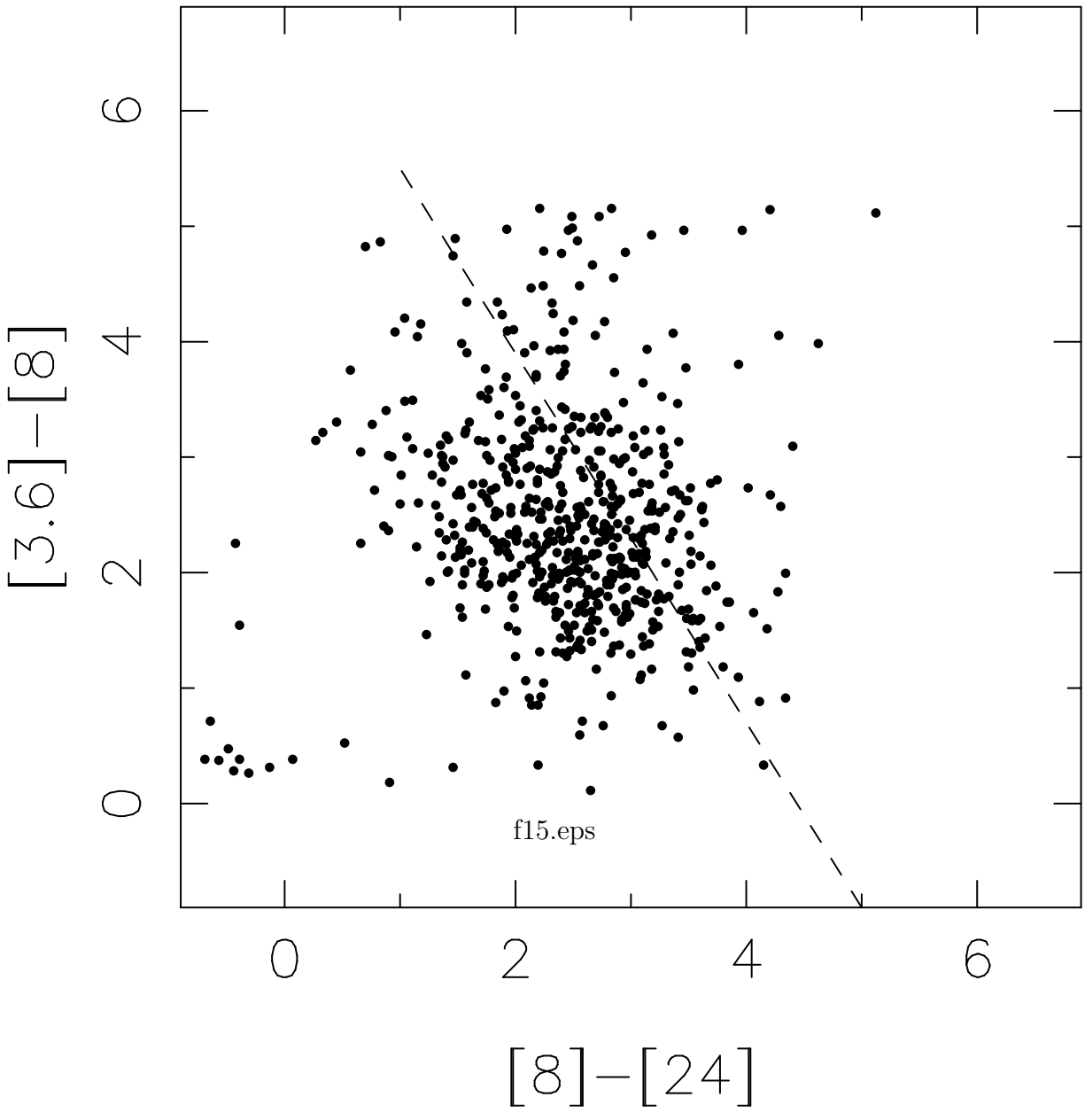
[3.6]−[8]
0
2
4
6
[8]−[24]
0
2
4
6
f15.eps

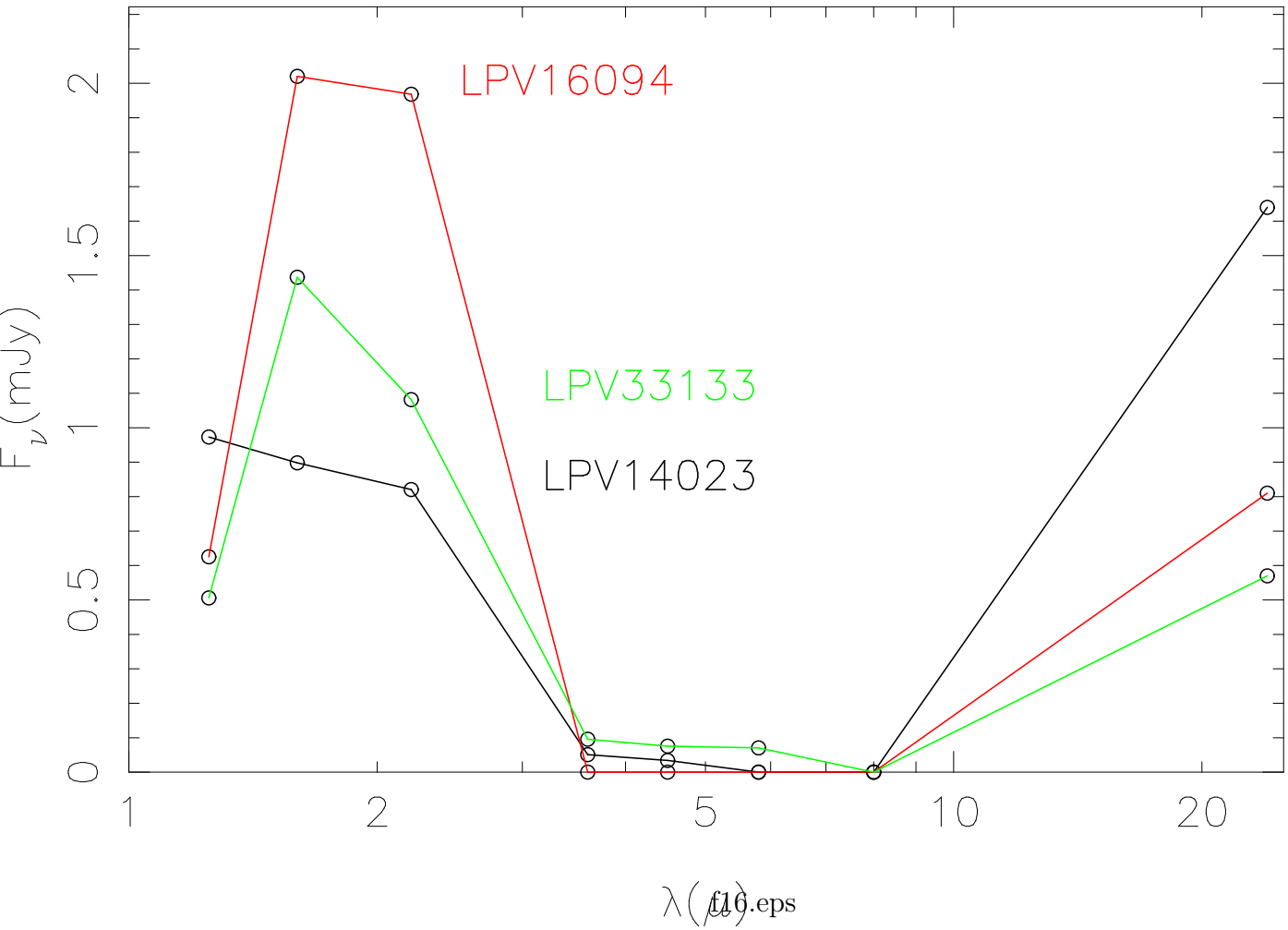

fig16.eps

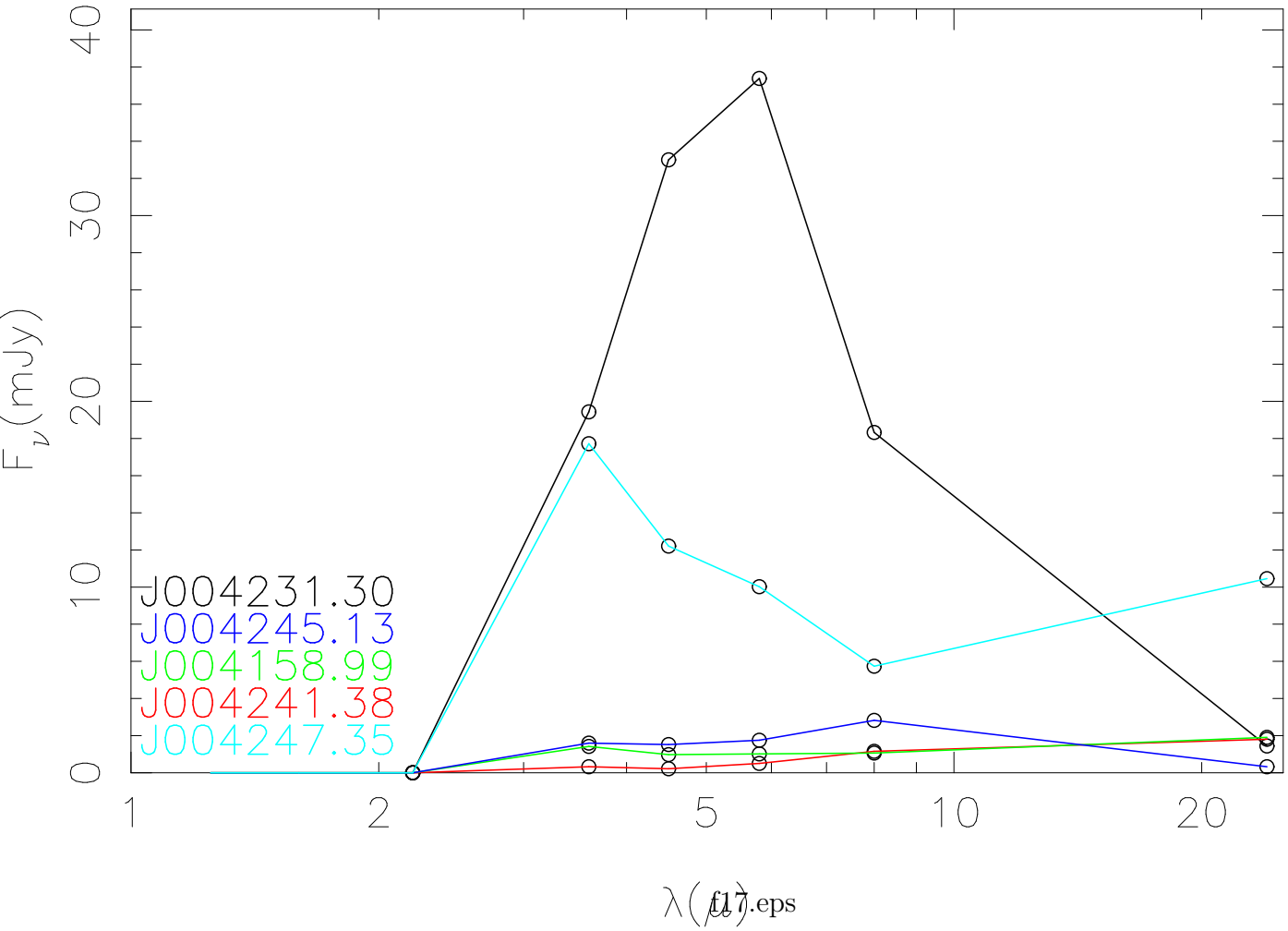
J004231.30
J004245.13
J004158.99
J004241.38
J004247.35
F_ν(mJy)
λ(μm)
0
10
20
30
40
1
2
5
10
20

fig17.eps

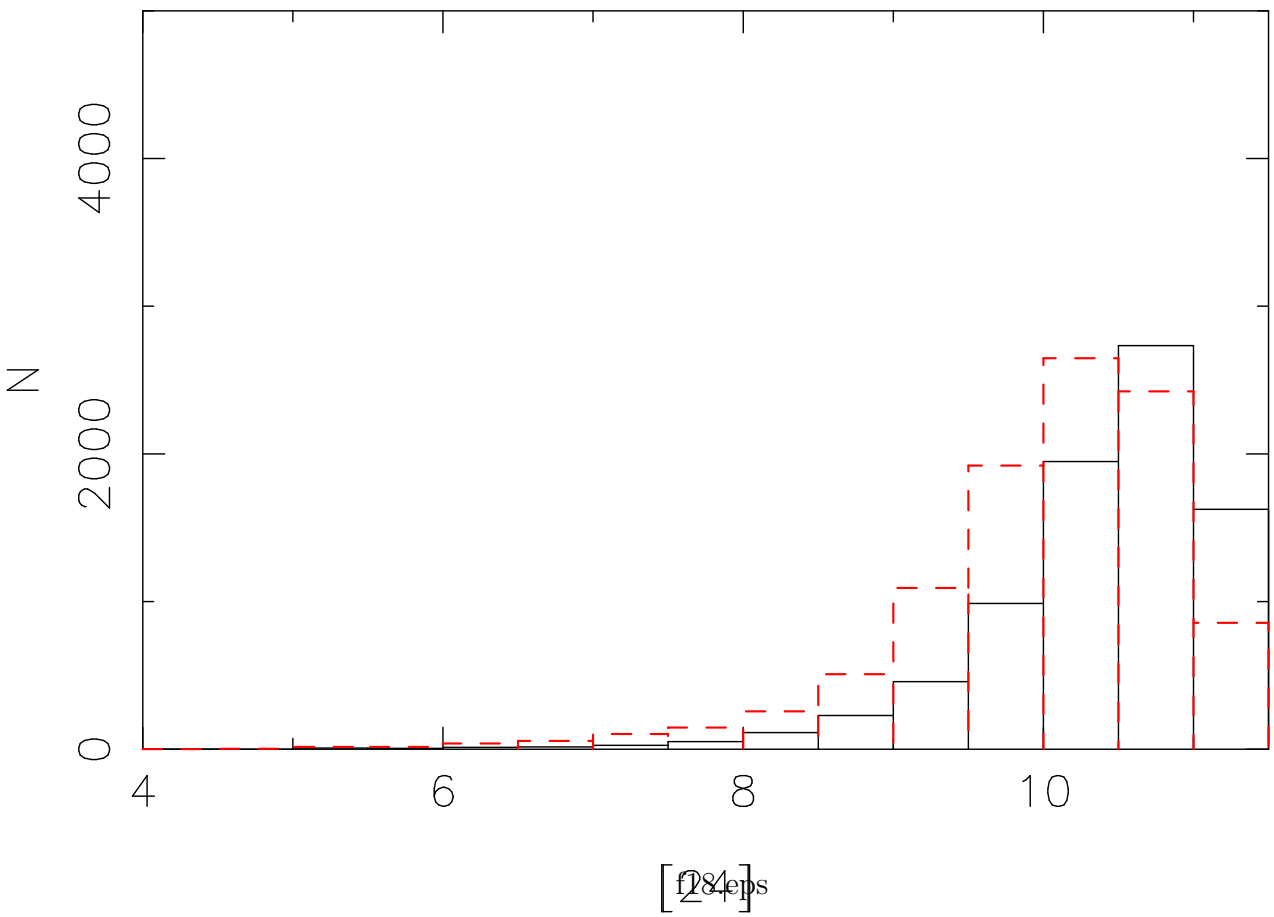

[f24eps]